Ultrafast field-resolved multi-THz spectroscopy on the sub-nanoparticle scale

Tyler L. Cocker*[a], Max Eisele[a], Markus A. Huber[a], Markus Plankl[a], Leonardo Viti[b], Daniele Ercolani[b], Lucia Sorba[b], Miriam S. Vitiello[b], Rupert Huber[a]

[a]Dept. of Physics, University of Regensburg, Universitätsstr. 31, 93040 Regensburg, Germany;
[b]NEST-CNR – Instituto Nanoscienze and Scuola Normale Superiore, Piazza San Silvestro 12, 56127 Pisa, Italy

ABSTRACT

Terahertz spectroscopy plays a key role in understanding ultrafast carrier dynamics in nanomaterials. Diffraction, however, limits time-resolved terahertz spectroscopy to ensemble measurements. By combining time-resolved terahertz spectroscopy in the multi-terahertz range with scattering-type near-field scanning optical microscopy, we show that we can directly trace ultrafast local carrier dynamics in single nanoparticles with sub-cycle temporal resolution (10 fs). Our microscope provides both 10 nm lateral resolution and tomographic sensitivity, allowing us to observe the ultrafast build-up of a local surface depletion layer in an InAs nanowire.

Keywords: Terahertz, THz, spectroscopy, ultrafast, near-field, nanoscopy, nanowire, sub-cycle

1. INTRODUCTION

Over the past 20 years, terahertz and multi-terahertz spectroscopy [1-16] have provided valuable insights into ultrafast carrier dynamics in nanomaterials. These techniques, referred to globally here as terahertz time-domain spectroscopy, use phase-stable ultrafast pulses to probe low-energy elementary excitations. Coherent detection of the terahertz electric-field waveform via, for example, electro-optic sampling, enables the extraction of both the real and imaginary parts of the dielectric function without the Kramers-Kronig relations [2-6]. By accessing the full complex conductivity directly, terahertz spectroscopy effectively provides two independent conductivity curves (the real and imaginary components) that can be compared to conductivity models to determine the physics of the system. The technique can also be extended to the transient conductivity stimulated by a pump pulse in what is called timeresolved terahertz spectroscopy. With a sufficiently broadband detector (e.g. an electro-optic crystal with a broad phase-matching bandwidth), the photoconductivity can even be determined at terahertz frequencies with time resolution faster than a single oscillation cycle of the terahertz probe pulse.

Nevertheless, despite the advantages of time-resolved terahertz spectroscopy, researchers have had to contend with the diffraction limit when investigating nanomaterials, restricting them to ensemble measurements of nano-objects. This has necessitated the use of various effective medium theories [2,3] to extract nanoscale information, which naturally introduces numerous fitting parameters and uncertainty into the conductivity curve fitting. More importantly, the properties of nanoparticles, nanocrystals and nanodomains can often depend drastically on size, structure, orientation and density. Such heterogeneity invariably leads to a smearing of their intrinsic responses when measurements are averaged over a large number of particles. In some cases this can even completely obscure interesting and important behavior.

Terahertz and multi-terahertz radiation can be combined with scanning probe microscopy techniques to overcome the diffraction limit and study single nanoparticles. Recently it was shown that a terahertz pulse can be used to drive an ultrafast current in a scanning tunneling microscope [17]. This enabled the observation of carrier capture into a single semiconductor nanoparticle. Another route to sub-wavelength spatial resolution is the detection of radiation scattered from the near field of an object [18-31]. Coherent, field-resolved detection of scattered pulses has been demonstrated at terahertz frequencies [18-20], but transient dynamics have not yet been explored. On the other hand, we recently demonstrated the first coherent detection of scattered multi-terahertz pulses and used our unique microscope to measure transient carrier dynamics on the 10 nm scale with sub-cycle (10 nm) temporal resolution [31].

Here, we demonstrate the capabilities of our ultrafast field-resolved multi-terahertz microscope. It is based on scattering-type near-field scanning optical microscopy (s-NSOM). We focus phase-stable multi-terahertz pulses onto the apex of the s-NSOM tip, where they experience significant field confinement and enhancement. The tip is operated in tapping mode, creating a modulation of the scattered multi-terahertz radiation that depends nonlinearly on the proximity of the tip apex to the sample surface. To efficiently isolate the local response of the sample from background scattering, the scattered radiation is detected at the harmonics of the tapping frequency. Detection at the third harmonic (often called the third demodulation order) provides 10 nm spatial resolution. We detect the scattered multi-terahertz radiation with two different techniques. The first is conventional intensity-resolved detection with a mercury cadmium telluride photodiode. This enables rapid imaging, measurements of the scattered intensity as a function of pump-probe delay time and Fourier transform infrared spectroscopy. Fourier transform infrared spectroscopy scans can be taken at

a particular pump-probe delay time to perform spectroscopy of the transient conductivity in the system. The time resolution of such a measurement is defined by the duration of the scattered multi-terahertz pulse, which is typically > 60 fs. These measurements reveal the amplitude spectrum of the scattered field transient (convoluted with the amplitude of the reference pulse) and the phase of the scattered pulse relative to the phase of the reference pulse. The second technique for the detection of scattered multi-terahertz radiation in our setup is electro-optic sampling. We use a GaSe crystal as a detector to maximize the phase-matching bandwidth of the multi-terahertz probe radiation relative to our near-infrared electro-optic gate pulse. This allows us to achieve a temporal resolution that is defined by the duration of the gate pulse, which is 10 fs. Since this is faster than an oscillation cycle of our multi-terahertz probe pulses (center frequency: 35 THz, full width at half maximum bandwidth: ~10 THz) we are able to map out the oscillating electric field of the pulses scattered from the near field and do spectroscopy with sub-cycle time resolution. The electric-near-field waveform that we measure originates from a $(10\ \mathrm{nm})^3$ volume at the surface of the sample. This spatial resolution is set by the radius of curvature of the sNSOM tip apex [22] (and the detection demodulation order) and was confirmed by electro-optic line scans [31].

In the following we show how our field-resolved multi-terahertz near-field microscope can be used to extract ultrafast nanoscopic information. We have applied our novel setup to the study of carrier dynamics in isolated indium arsenide (InAs) nanowires: (i) Ultrafast intensity-resolved imaging provides a map of the photoinduced carrier density. (ii) Field-resolved nano-spectroscopy at a particular point on the nanowire quantitatively reveals the local evolution of the plasma frequency with sub-cycle time resolution.

2. RESULTS

The sample consisted of InAs nanowires [32-34] on a diamond substrate. The nanowires were grown bottom-up on InAs (111)B substrates by chemical beam epitaxy using gold particles as a growth catalyst. Selenium incorporation provided the nanowires with *n*-type doping ($N_c \sim 2 \times 10^{17}\ \mathrm{cm}^{-3}$). After growth the nanowires were mechanically transferred to the diamond substrate. The large-area atomic force microscope topography scan in Fig. 1a shows a number of isolated nanowires, and even some pairs of overlapping nanowires. Scattered near-field multi-terahertz intensity I_3 images (measured at the third demodulation order) are shown in Fig. 1b and 1c. The difference between the images is due to ultrafast excitation by a near-infrared pump pulse (1550 nm, 22 fs). The image in Fig. 1b was taken at a pump-probe delay time of t_{pp} = -5 ps, and therefore shows no effects of photoexcitation. In Fig. 1c, on the other hand, the pump pulse arrives 50 fs before the multi-terahertz probe pulse (t_{pp} = 50 fs), which subsequently scatters from the nanowire when it is in a photoexcited state. Notably, the scattering response from the different nanowires is not uniform. This contrast is a direct consequence of the different densities of photoexcited carriers in the different nanowires. (Far-field measurements would average over these variations.)

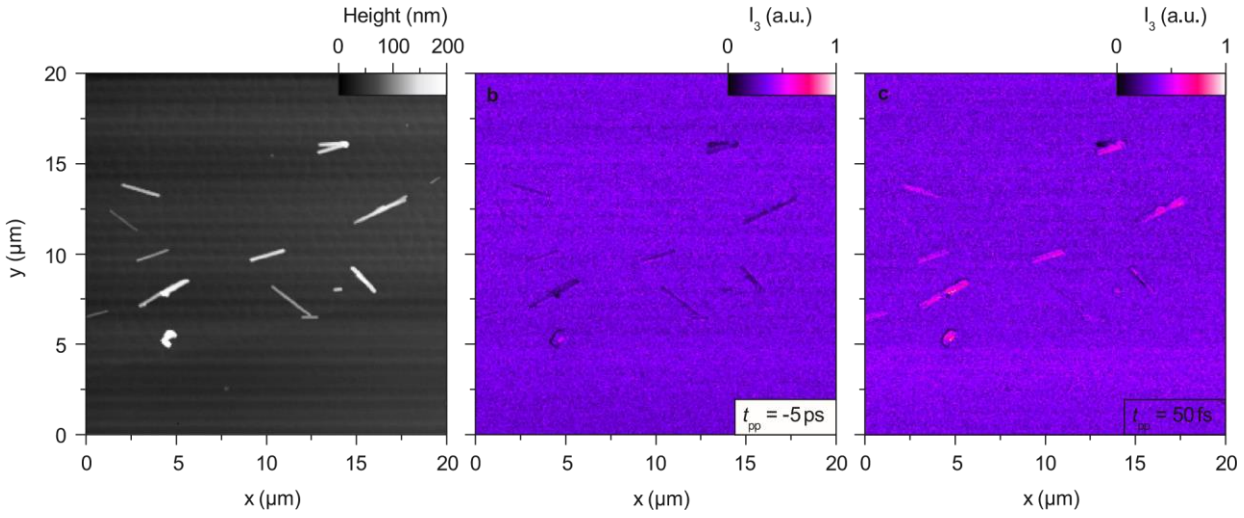

Figure 1: Ultrafast near-field imaging of indium arsenide (InAs) nanowires. a, Topography of InAs nanowires on a diamond substrate measured by atomic force microscopy. Dashed box: imaging region for Fig. 2. **b**, Scattered near-field multi-terahertz intensity recorded at the third harmonic of the tip tapping frequency (I_3) for negative pumpprobe delay ($t_{pp} < 0$ ps). **c**, Multi-terahertz near-field image recorded at positive pump-probe delay (t_{pp} = 50 fs). At positive delay the near-infrared (1550 nm, 22 fs) pump pulses photoexcite free electron-hole pairs in the nanowires and the multi-terahertz pulses subsequently probe the local transient dielectric function. When the plasma frequency of the free carriers in a nanowire exceeds the center frequency of the multi-THz pulse, the scattered multi-terahertz near-field intensity is greatly enhanced.

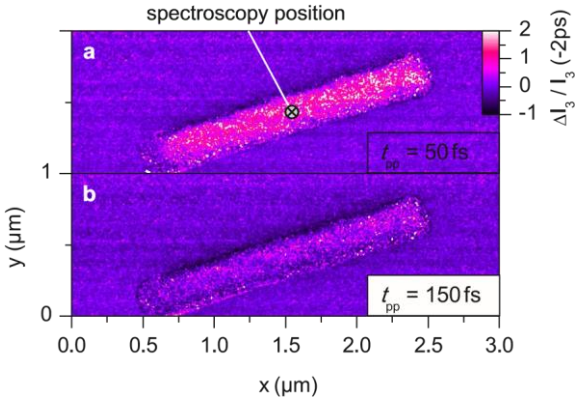

Figure 2: Differential ultrafast near-field imaging. a, Relative change to the scattered near-field intensity (I_3) measured at t_{pp} = 50 fs compared to that recorded at negative delay (t_{pp} = -2 ps) for the InAs nanowire in the center of Fig. 1. Since the local multi-terahertz scattering response is determined by the instantaneous plasma frequency, a differential image provides a (nonlinear) map of the local photoinduced carrier density. **b**, Differential multiterahertz near-field image recorded at a pump-probe delay of t_{pp} = 150 fs. Differences between **a** and **b** are caused by dynamics on the < 100 fs time scale. The spectroscopy data in Fig. 3 was taken at the position marked in **a**.

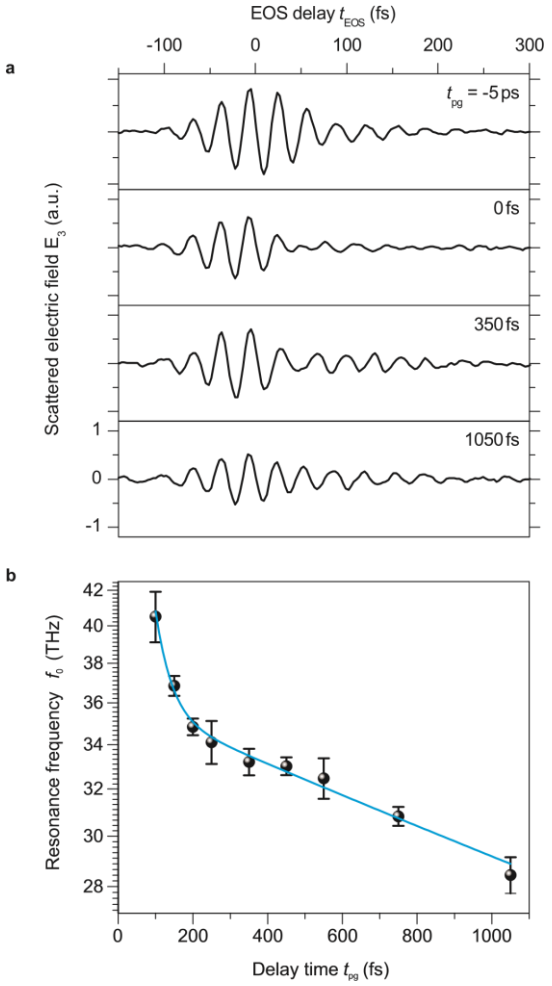

Figure 3: Field-resolved multi-terahertz nano-spectroscopy on the surface of an InAs nanowire. a, Multiterahertz electric-field waveforms scattered from the center of the InAs nanowire in Fig. 2 (spectroscopy position) measured by electro-optic sampling at the third harmonic of the tip tapping frequency (E_3, spatial resolution = 10 nm). As the delay between the near-infrared pump pulse and electro-optic gate pulse (t_{pg}) is changed, the multiTHz transients are significantly modified due to the shift of a resonance through the probe spectrum. **b**, The resonance frequency corresponds to the local plasma frequency in a $(10\ nm)^3$ volume of the InAs nanowire, and hence its decay as a function of time after photoexcitation shows the evolution of the local carrier density with subcycle temporal resolution. Black points: experimental resonance frequency; blue line: biexponential decay (fit to data) with time constants of 40 fs and 3.5 ps.

The differential response of the nanowire in the center of the images in Fig. 1 (dashed area) is shown in Fig. 2 for two different pump-probe delay times, t_{pp} = 50 fs (Fig. 2a) and t_{pp} = 150 fs (Fig. 2b). We note that while ultrafast effects induced by pumping are often detected directly in differential mode, here we subtract an intensity-resolved image taken before excitation from each one taken after excitation (e.g. subtracting Fig. 1b from Fig. 1c) and divide the result by the unpumped image to avoid measurement artefacts due to the thermal response of the s-NSOM tip. The increase in the relative strength of the local near-field scattering observed in Fig. 2 is due to the shift of the local plasma frequency through our multi-terahertz probe bandwidth. This shift is the direct result of photogenerated free carriers since the square of the plasma frequency is proportional to the carrier density. Therefore, the relative change to the scattered near-field intensity in Fig. 2 provides a map of the photogenerated free carriers, albeit with a nonlinear scale, and the spatial variations of $\Delta I_3(t_{pp})/I_3(\text{-}2\text{ ps})$ are the result of local differences in photoinduced carrier density. The contrast at the ends of the nanowire in Fig. 2a is of particular interest. The low photocarrier density at the bottom left end of the nanowire directly following excitation may indicate that this is the 'start' of the nanowire, where a gold catalyst droplet initialized growth. Conversely, while the carrier density immediately following photoexcitation is homogeneously distributed along the wire (except the bottom left), some areas decay faster within 100 fs. The < 100 fs decay is due to the formation of a carrier depletion layer [31], so a faster decay in some regions could signify a thicker depletion layer in these areas, which may result from inhomogeneities in the selenium doping concentration or curvature of the nanowire surface at the edges.

The evolution of the local plasma frequency is most accurately resolved by ultrafast field-resolved multi-terahertz nano-spectroscopy. To do this, the tip was placed in the center of the nanowire in Fig. 2 (spectroscopy position) and the scattered multi-terahertz electric field was measured at the third harmonic of the tapping frequency (E_3), as shown in Fig. 3a. This waveform, which corresponds to the oscillating electric field from a $(10\text{ nm})^3$ volume on the nanowire surface [31], changes significantly as a function of delay after photoexcitation t_{pg}. The most drastic differences occur in the trailing oscillations of the transient—the (effective) free induction decay of the plasma frequency. The plasma resonance frequency is plotted as a function of delay time after photoexcitation in Fig. 3b on a log-linear plot. It follows a biexponential decay with time constants of 40 fs and 3.5 ps. These decays correspond to the formation of a carrier depletion layer and carrier trapping into surface defect states, respectively [31]. The faster of these two dynamics occurs on a time scale comparable to a single oscillation cycle of the multi-terahertz probe light, highlighting the strength of field-resolved detection.

3. CONCLUSIONS

We have demonstrated ultrafast near-field imaging of InAs nanowires and field-resolved pump-probe multi-terahertz spectroscopy on the surface of an InAs nanowire. We have extracted the local plasma frequency from a $(10\text{ nm})^3$ volume with 10 fs time resolution, faster than a single oscillation cycle of the multi-terahertz probe. These results herald the start of a new era for sub-cycle multi-terahertz spectroscopy wherein dynamics can be probed *within* a wide variety of single nanoparticles. Ultrafast field-resolved nanoscopy also opens the door to nonlinear near-field terahertz control [35,36] of individual nano-systems.

REFERENCES

[1] Kampfrath, T., Tanaka, K. and Nelson, K. A. "Resonant and nonresonant control over matter and light by intense terahertz transients," Nature Photon. **7**, 680 (2013).

[2] Lloyd-Hughes, J. and Jeon, T.-I. "A Review of the Terahertz Conductivity of Bulk and Nano-Materials," J. Infrared Milli. Terahz Waves **33**, 871 (2012).

[3] Ulbricht, R., Hendry, E., Shan, J., Heinz, T. F. and Bonn, M., "Carrier dynamics in semiconductors studied with time-resolved terahertz spectroscopy," Rev. Mod. Phys. 83, 543 (2011).

[4] Jepsen, P. U., Cooke, D. G. and Koch, M. "Terahertz spectroscopy and imaging – Modern techniques and applications," Laser Photon. Rev. **5**, 124 (2011).

[5] Kindt, J. T. and Schmuttenmaer, C. A., "Theory for determination of the low-frequency time-dependent response function in liquids using time-resolved terahertz pulse spectroscopy," J. Chem. Phys. 110, 8589 (1999).

[6] Huber, R. *et al*., "How many-particle interactions develop after ultrafast excitation of an electron-hole plasma," Nature 414, 286 (2001).

[7] Kaindl, R. A., Carnahan, M. A., Hägele, D., Lövenich, R. and Chemla, D. S., "Ultrafast terahertz probes of transient conducting and insulating phases in an electron-hole gas," Nature 423, 734 (2003).

[8] Baxter, J. B. and Schmuttenmaer, C. A., "Conductivity of ZnO nanowires, nanoparticles, and thin films using time-resolved terahertz spectroscopy," J. Phys. Chem. B 110, 25229 (2006).

[9] Wang, F. *et al*., "Exciton polarizability in semiconductor nanocrystals," Nature Mater. 5, 861-864 (2006). [10] Kübler, C. *et al*., "Coherent structural dynamics and electronic correlations during an ultrafast insulator-to- metal phase transition in VO_2," Phys. Rev. Lett. 99. 116401 (2007).

[11] Gaal, P. *et al*., "Internal motions of a quasiparticle governing its ultrafast nonlinear response," Nature 458, 1210 (2007).
[12] Günter, G. *et al*., "Sub-cycle switch-on of ultrastrong light-matter interaction," Nature 458, 178-181 (2009).
[13] Pashkin, A. *et al*., "Femtosecond response of quasiparticles and phonons in superconducting $YBa_2Cu_3O_{7-\delta}$ studied by wideband terahertz spectroscopy," Phys. Rev. Lett. 105, 067001 (2010).
[14] Liu, M. K. *et al*., "Photoinduced phase transitions by time-resolved far-infrared spectroscopy in V_2O_3," Phys. Rev. Lett. 107, 066403 (2011).
[15] Seletskiy, D. V. *et al*., "Efficient terahertz emission from InAs nanowires," Phys. Rev. B 84, 115421 (2011).
[16] Joyce, H. J. *et al*., "Electronic properties of GaAs, InAs and InP nanowires studied by terahertz spectroscopy," Nanotechnology 24, 214006 (2013).
[17] Cocker, T. L. *et al*., "An ultrafast terahertz scanning tunnelling microscope," Nature Photon. 7, 620 (2013).
[18] Chen, H.-T., Kersting, R. and Cho, G. C., "Terahertz imaging with nanometer resolution," Appl. Phys. Lett. 83, 3009-3011 (2003).
[19] Zhan, H. *et al*., "The metal-insulator transition in VO_2 studied using terahertz apertureless near-field microscopy," Appl. Phys. Lett. 91, 162110 (2007).
[20] Moon, K. *et al*., "Quantitative coherent scattering spectra in apertureless terahertz pulse near-field microscopes," Appl. Phys. Lett. 101, 011109 (2012).
[21] Qazilbash, M. M. *et al*., "Mott transition in VO_2 revealed by infrared spectroscopy and nano-imaging," Science 318, 1750-1753 (2007).
[22] Jones, A. C. *et al*., "Mid-IR plasmonics: near-field imaging of coherent modes of silver plasmon modes of silver nanowires," Nano Lett. 9, 2553-2558 (2009).
[23] Stiegler, J. M. *et al*., "Nanoscale Free-Carrier Profiling of Individual Semiconductor Nanowires by Infrared Near-Field Nanoscopy," Nano Lett. **10**, 1387 (2010).
[24] Diyar, S. *et al*., "Adiabatic nanofocusing scattering-type optical nanoscopy of individual gold nanoparticles," Nano Lett. 11, 1609-1613 (2011).
[25] Krutokhvostov, R. *et al*., "Enhanced resolution in subsurface near-field optical microscopy," Opt. Express 20, 593-600 (2012).
[26] Chen, J. *et al*., "Optical nano-imaging of gate-tunable grapheme plasmons," Nature 487, 77-81 (2012). [27] Fei, Z. *et al*., "Gate-tuning of graphene plasmons revealed by infrared nano-imaging," Nature 487, 82-85 (2012).
[28] Jacob, R. *et al*., "Intersublevel spectroscopy on single InAs-quantum dots by terahertz near-field microscopy," Nano Lett. 12, 4336-4340 (2012).
[29] Westermeier, C. *et al*., "Sub-micron phase coexistence in small-molecule organic thin films revealed by infrared nano-imaging," Nat. Commun. **5**, 4101 (2014).
[30] Wagner, M. *et al*., "Ultrafast and nanoscale plasmonic phenomena in exfoliated graphene revealed by infrared pump-probe nanoscopy," Nano Lett. 14, 894-900 (2014).
[31] Eisele, M. *et al*., "Ultrafast multi-terahertz nano-spectroscopy with sub-cycle temporal resolution," Nature Photon. **8**, 841 (2014).
[32] Vitiello, M. S. *et al*., "Room-temperature terahertz detectors based on semiconductor nanowire field-effect transistors," Nano Lett. 12, 96-101 (2012).
[33] Saxena, D. *et al*., "Optically pumped room-temperature GaAs nanowire lasers," Nature Photon. 7, 963-968 (2013).
[34] Mayer, B. *et al*., "Lasing from individual GaAs-AlGaAs core-shell nanowires up to room temperature," Nature Commun. 4, 2931 (2013).
[35] Schubert, O. *et al*., "Sub-cycle control of terahertz high-harmonic generation by dynamical Bloch oscillations," Nature Photon. **8**, 119 (2014).
[36] Hohenleutner, M. *et al*., "Real-time observation of interfering crystal electrons in high-harmonic generation," Nature **523**, 572 (2015).

*tyler.cocker@ur.de